

3D Object Classification on Partial Point Clouds: A Practical Perspective

Zelin Xu*, Ke Chen*, Tong Zhang, C. L. Philip Chen, and Kui Jia[†]
South China University of Technology

eexuzelin@mail.scut.edu.cn, {chenk, tony, philipchen, kuijia}@scut.edu.cn

Abstract

A point cloud is a popular shape representation adopted in 3D object classification, which covers the whole surface of an object and is usually well aligned. However, such an assumption can be invalid in practice, as point clouds collected in real-world scenarios are typically scanned from visible object parts observed under arbitrary $SO(3)$ viewpoint, which are thus incomplete due to self and inter-object occlusion. In light of this, this paper introduces a practical setting to classify partial point clouds of object instances under any poses. Compared to the classification of complete object point clouds, such a problem is made more challenging in view of geometric similarities of local shape across object classes and intra-class dissimilarities of geometries restricted by their observation view. We consider that specifying the location of partial point clouds on their object surface is essential to alleviate suffering from the aforementioned challenges, which can be solved via an auxiliary task of 6D object pose estimation. To this end, a novel algorithm in an alignment-classification manner is proposed in this paper, which consists of an alignment module predicting object pose for the rigid transformation of visible point clouds to their canonical pose and a typical point classifier such as PointNet++ and DGCNN. Experiment results on the popular ModelNet40 and ScanNet datasets, which are adapted to a single-view partial setting, demonstrate the proposed method can outperform three alternative schemes extended from representative point cloud classifiers for complete point clouds.

1. Introduction

The problem of object classification in the 3D domain aims to categorize object shape into semantic classes according to their global topological configuration of local geometry primitives. A point cloud is a popular shape representation in 3D object classification owing to its simple structure and easy acquisition as the raw output of 3D scan-

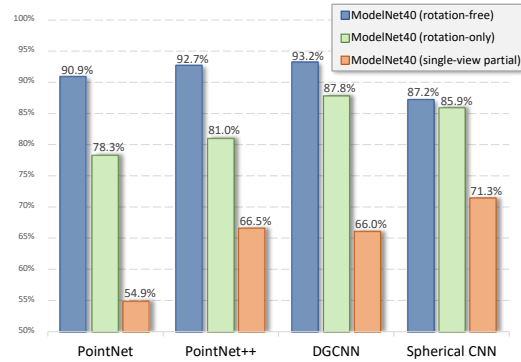


Figure 1. Comparative results of four popular point cloud classifiers, *i.e.* PointNet [23], PointNet++ [24], DGCNN [35] and Spherical CNN [9], with three settings. Compared to ideal rotation-free (in blue) and rotation-only (in green) settings, our single-view partial setting (in orange) is more challenging in view of partially visible point clouds and pose variations, which makes classification accuracy of all four classifiers decrease with a significant margin. Results are reported on the ModelNet40 for the rotation-free and rotation-only settings and its partial variant – PartialModelNet40 for the proposed single-view partial setting.

ners such as the LiDAR in real-world applications. A large number of deep networks such as PointNet [23], PointNet++ [24], and DGCNN [35] have been developed to handle data-specific challenges – sparsity and irregularity of the point cloud representation, which is under an ideal condition where point clouds are uniformly sampled from the whole surface of object CAD instances aligned in category-level canonical poses¹ [37, 3, 25].

Towards a practical setting, *i.e.* relaxing the strict rotation-free assumption on object instances to the arbitrarily posed one, most of the existing convolutional operations on point clouds can have a fundamental challenge that their output of feature representations is sensitive to rotation changes. In light of this, recent rotation-agnostic works concern with eliminating the negative effects of such pose variations. Rotation invariance can be achieved by either learning rotation-invariant feature representation [4, 44, 42], learning rotation-equivariant features via Spherical Fourier

*Equal contributions

[†]Corresponding author

¹In the ModelNet40 [37], object instances are tolerant of having any arbitrary rotation only along the Z -axis.

Transform [6, 9] or explicit shape alignment via weakly supervised spatial transformation [23, 35, 43]. Although these methods all agree that the poses of object models, where point clouds obtained from, are often uncontrollable in practice, their point cloud representation is typically complete and uniformly sampled via the Farthest Point Sampling (FPS) [24].

In a more practical perspective, point clouds residing in the real-world environment are incomplete due to interaction with cluttered contextual objects and self-occlusion restricted by limited observation viewpoints. In other words, only *partial* surface can be observed, and thus point clouds can only be scanned from those visible regions. In this work, we are motivated to extend recent interests of rotation-only point set classification to such a more practical scenario. Specifically speaking, *partial* and *unaligned* point clouds in our setting can significantly increase difficulties of semantic classification in two folds – inter-class similarity and intra-class dissimilarity of local shapes, in comparison with the existing settings. On one hand, different semantic classes can share common parts, which can lead to geometrically similar point clouds from local regions belonging to different categories. On the other hand, due to limited observation angles, the partially visible surface spatially varies within the whole shape. Therefore the shape of the partial surface may not uniquely characterize object semantics. It is worth pointing out that classifying aligned partial point clouds is very similar to the rotation-free setting of complete point clouds, as both settings have consistent intra-class geometries from the unique canonical viewing angle.

We compare a number of existing representative point set classifiers under the proposed single-view partial setting² as well as existing settings on well-aligned (*i.e.* rotation-free) and unaligned (*i.e.* rotation-only) point sets from a complete object surface, whose results visualized in Figure 1 verify that their performance can be degraded drastically due to partial observations compounded with unconstrained poses. As the category of a surface shape is defined by a global, topological configuration of local shape primitives, point cloud classification under the partial, arbitrarily posed setting is less ambiguous only when the distribution of the partial surface on the complete one is clearly specified. To this end, the problem of partial point cloud classification demands localization of partial shapes on the whole surface as an auxiliary target. Evidently, such a localization problem can be formulated into a supervised regression problem of estimating a rigid transformation (*i.e.* 6D pose) to a category-level canonical rotation and translation. Consequently, partial point cloud representations after the transformation can readily associate with spatially-distributed

²We denote the proposed setting of classifying partially observed and arbitrarily posed point clouds as the single-view partial setting for simplicity.

object parts to alleviate inter-class ambiguities and also large intra-class variations. Note that, we assume that object instances have been detected from contexts, which differentiates our setting from amodal 3D object detection [10, 27], by focusing more on learning semantics from object surface geometries instead of precisely locating objects in the 3D space.

This paper proposes an end-to-end learning pipeline which consists of two modules – 6D pose estimation based shape alignment and point cloud classification. The former is fed with partial point clouds as an input and predicts their 6D poses to align the input point set into a canonical space to make subsequent point cloud classification easier. The latter adopts any off-the-shelf point set classifier (*e.g.* PointNet [23], PointNet++ [24], DGCNN [35]) to digest the transformed point clouds to output their class predictions. To benchmark our method and alternative solutions extended from the popular classifiers, we adapt the synthetic ModelNet40 [37] and the realistic ScanNet [7] to the single-view partial setting, where our method can consistently achieve superior classification performance. The main contributions of this paper are as follows:

- This paper introduces a realistic single-view partial setting of point cloud classification, which introduces more challenges of point set classification, *i.e.* inter-class similarity and large intra-class variations of partially observed and arbitrarily posed geometries.
- This paper reveals that specifying the distribution of partial point clouds on the object surface can alleviate semantic ambiguities, which encourages us to propose a new classification algorithm with an auxiliary task of object pose estimation.
- Experiment results on two partial point cloud classification datasets can verify our motivation and superior performance to several alternative solutions based on popular complete point cloud classifiers.

Datasets, source codes, and pre-trained models will be released at <https://github.com/xziscut/PartialPointClouds>.

2. Related Works

Object Classification on Point Sets – As a pioneer, the PointNet [23] starts the trend of designing deep networks for operating on irregular point-based surface but misses considering geometric patterns in local regions to benefit semantic analysis, which encourages a number of recent works including point-wise MLP-based methods [24, 17, 41, 46, 8, 40], convolutional algorithms [18, 9, 15, 29, 16], and graph-based methods [35, 26, 4]. Recently, the problem of rotation-agnostic classification on point clouds has attracted wide attention, which imposes rotation equivariance or invariance into feature learning with respect to

pose transformations. A number of methods have been proposed to either exploit local geometric features invariant to rigid rotation transformation [4, 44, 42], or exploit group transformation actions to learn rotation equivariant features [6, 9], or even learning with explicit transformation [23, 35, 43]. All these rotation-agnostic methods can be readily applied to our single-view partial setting (more technical details are given in Sec. 4), but cannot perform well without any knowledge about the configuration of observed shape on the whole object surface (See Table 1 in Sec. 7).

Point Classification Towards Real-World Data – Compared to synthetic point clouds sampled from object CAD models, real-world point clouds are typically incomplete and unaligned in addition to irregularly distribution of points such as the existence of holes. Very few existing works [32, 43] have explored to handle with the compound challenges of rotation variations and partially visible shape. Uy *et al.* [32] propose a realistic point cloud classification benchmark, whose setting is similar to ours, but the main differences lie in two folds. On one hand, object shapes in the ScanObjectNN [32] only have arbitrary rotations along the vertical axis, instead of the $SO(3)$ rotation group containing all possible rotation transformations in \mathbb{R}^3 in our setting. On the other hand, point clouds in the ScanNet [7] and SceneNN [12] were obtained via fusion of a depth image sequence with multiple viewpoints, and thus objects segmented by the ScanObjectNN [32] in these two datasets can not reflect single-view partiality in real data. Consequently, although both methods are interested in semantic analysis on partial point clouds, their method concerns more on robust classification performance with noisy point cloud input, while our method treats pose variations as the main challenge. Yuan *et al.* [43] share a similar observation on realistic point cloud classification to handle with partial and unaligned point clouds, which designs an iterative transformation network (ITN) to align partial point clouds before they are fed into a classification module. The ITN [43] in principle searches the $SO(3)$ space for a set of optimal centers in pose space that makes partial shape after transformation easier to classify, and therefore its transformation module is directly supervised by its final classification goal. The weakly supervised pose transformation in ITN can be less effective in coping with visually similar partial point clouds from different classes due to the lack of their specific distribution on the object surface. In contrast, our method focuses on localizing partial shape on the whole surface, which can be clearly defined in a category-level canonical space. As a result, supervised regressing on object pose is treated as a proxy task to specify the locations of shape primitives, whose aligned shape can be readily obtained via rigid pose transformation. Experiments in Sec. 7 verify the superior performance of our method to the ITN.

6D Pose Estimation – The problem of 6D pose estimation aims to predict object poses (*i.e.* a rotation and translation) in the camera space according to canonical pose space. Existing 6D pose estimation can be categorized into two groups – instance-level [38, 19, 33, 39] and category-level [34, 5, 31]. In instance-level 6D pose estimation [38, 19, 33, 39], a typical assumption is adopted that CAD models for object instances to be estimated are available. In this sense, these methods concern more on learning to match partial observation to the CAD model without considering shape changes across instances. In category-level 6D pose estimation [34, 5, 31], without CAD models of each instance during testing, such a problem is made more challenging to cope with shape variations of unseen object instances and thus relies on a high-quality category-level mean shape. The object pose estimator in our method falls into the latter group but does not estimate the size of object instances compared to existing category-level pose estimators. The rational explanation is the main task of partial point classification will normalize all input point cloud into a unit ball, rather than object detection in [34, 5, 31]. Existing works on category-level 6D pose employ the MLP-based feature encoding, which is less effective to reveal rotation changes. Such an observation encourages us to use Spherical CNN [9] as the backbone encoder for object pose estimation in our scheme, which can perform better (see Table 3 in Sec. 7).

3. Problem Definition

For the conventional point set classification with \mathcal{X}_c and \mathcal{Y} denoting the input and output space, given N_s training samples, each consisting of a complete point cloud $\mathcal{P}_c = \{\mathbf{p}_i \in \mathbb{R}^3\}_{i=1}^{N_c} \in \mathcal{X}_c$ of N_c points and its corresponding category label $y \in \mathcal{Y}$, where the size of object classes $|\mathcal{Y}| = K$, the goal is to learn a mapping function $\Phi_c : \mathcal{X}_c \rightarrow \mathcal{Y}$ that classifies \mathcal{P}_c into one of the K categories. Note that, each object CAD instances, where a point cloud are generated from, can be well aligned to either the canonical pose as [24, 35] or arbitrarily posed at $[\mathbf{R}|\mathbf{t}]$ w.r.t. a category-level canonical pose as [4, 9], where $\mathbf{R} \in SO(3)$ and $\mathbf{t} \in \mathbb{R}^3$.

Plenty of recent methods propose deep models to classify point clouds of complete object surface [23, 24, 35, 17], but they focus on objects under canonical poses. Although the scale and translation variation can be eliminated by normalizing the input point cloud to a unit sphere, these methods are by design rotation-dependent, and as such, arbitrarily rotated object point clouds would degrade the performance of these methods. This is certainly undesirable considering the fact that complete surface shapes of an object captured at different poses represent the same geometric and semantic pattern. The issue motivates recent proposals of rotation-agnostic methods [4, 9, 43], whose designs are generally based on the following three strategies. Technical

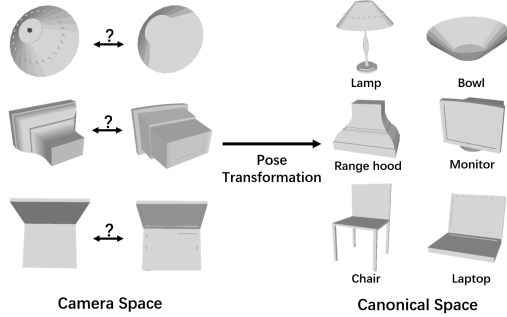


Figure 2. Illustration of ambiguous examples of inter-class similarity of partially observed shapes on the ModelNet40 [37]. Three pairs of shape primitives from different classes on the left are visually similar to each other, but they are distinguishable after pose transformation to a canonical space on the right.

details of these strategies are given in Sec. 4.

Although the problem of rotated point cloud classification has considered to alleviating negative effects of pose changes, however, these methods are not directly relevant to the single-view partial setting considered in this work, which extends recent interests of classifying point clouds from a *complete* object surface [37] to a more practical scenario, *i.e.* the point representation is incomplete due to self and inter-object occlusions and un-aligned (*i.e.* under any rotation group $SO(3)$). In this sense, the input and output of training pair of each instance consists of a point cloud $\mathcal{P} = \{\mathbf{p}_i \in \mathbb{R}^3\}_{i=1}^N \in \mathcal{X}$ of N points covering a *partially visible* surface of an object arbitrarily posed at $[\mathbf{R}|\mathbf{t}]$, together with its class label $y \in \mathcal{Y}$. We study learning a prediction function $\Phi : \mathcal{X} \rightarrow \mathcal{Y}$ to categorize \mathcal{P} into one of K semantic classes.

As noted in Sec. 1, the category of a surface shape is defined by a global, topological configuration of local shape primitives; more precisely, the category of a surface shape can be determined only when both the geometric patterns of its local shape primitives and their global configuration in the 3D space are specified. In Figure 2, we illustrate a number of ambiguous example pairs, each pair of which from different object classes can be visually similar under specific viewing angles but can be easily distinguished from other poses (*e.g.* the pre-defined category-level canonical poses). Moreover, an unknown partial surface is difficult to define a unique object category, except in special cases in which surface parts unique to specific categories are observed. As such, our considered partial setting drastically improves the difficulty of recognizing geometric patterns when compared with the complete setting considered in the recent research [37]. As shown in Figure 1, when arbitrarily rotation and partial observation are compounded, the classification accuracy of four recent benchmarking baselines decreases at least 14.5%. Nevertheless, existing rotation-agnostic methods perform robustly against rotation variations, and we are thus interested in applying these methods

in the considered partial setting by investigating their efficacy to cope with pose variations (See Sec. 7).

The above analysis suggests that given a partially observed object surface, its category is less ambiguous only when where the observed surface part is located on the whole surface is clear. This requirement translates as predicting the object pose from the partial surface observation. We thus argue for *supervised pose regression* as an auxiliary task in order to benefit the subsequent task of classifying partial point sets. The specifics are given in Sec. 5.

4. Limitations of Alternative Solutions

Rotation-agnostic methods achieve invariance to rotation using the following strategies. Denote $\Phi_{fea} : \mathbb{R}^{N \times 3} \rightarrow \mathbb{R}^d$ as the feature encoding module, which produces d -dimensional feature embedding $\Phi_{fea}(\mathcal{P})$ for any input \mathcal{P} , and $\Phi_{cls} : \mathbb{R}^d \rightarrow [0, 1]^K$ as the final classifier typically constructed by fully-connected layers. These methods implement point set classification as a cascaded function $\Phi = \Phi_{cls} \circ \Phi_{fea}$. We briefly discuss how they instantiate Φ_{fea} .

Learning Rotation-Invariant Feature Representations

– Rotation-invariant learning requires that $\Phi_{fea}(\mathbf{R}\mathcal{P}) = \Phi_{fea}(\mathcal{P})$ for any $\mathbf{R} \in SO(3)$. It can be easily shown that the geometric quantities of point-wise norm and angle between a pair of points are rotation-invariant, *i.e.* $\|\mathbf{R}\mathbf{p}\|_2 = \|\mathbf{p}\|_2$ and $\langle \mathbf{R}\mathbf{p}, \mathbf{R}\mathbf{p}' \rangle = \langle \mathbf{p}, \mathbf{p}' \rangle, \forall \mathbf{p}, \mathbf{p}' \in \mathbb{R}^3$. Higher-order geometric quantities invariant to rotation can be obtained by constructing local neighborhoods around each $\mathbf{p} \in \mathcal{P}$, which altogether provide rotation-invariant input features for subsequent learning via graph networks [24, 35]. Rotation-invariant feature learning methods [4, 44, 42, 45] thus implement Φ_{fea} by learning point-wise features from these invariant inputs, followed by pooling in a hierarchy of local neighborhoods constructed by graph networks; as such, they produce $\Phi_{fea}(\mathcal{P}) \in \mathbb{R}^d$. Pre-aligning \mathcal{P} globally to a canonical pose via alignment of PCA axes may also be used to improve the invariance [45]. However, using hand-crafted geometric quantities as point-wise descriptor may not be optimal. Repeatability of the reference axis or the local reference frame directly affects the invariance and robustness of the input descriptor [20, 21].

Achieving Rotation Invariance via Learning Rotation-Equivariant Deep Features

– Rotation invariance can also be achieved by first learning rotation-equivariant deep features and then pooling the features over the rotation group $SO(3)$. Typical methods of such a kind are spherical CNNs [6, 9]. Denote a rotation-equivariant layer as $\Psi : SO(3) \times \mathbb{R}^{d_{in}} \rightarrow SO(3) \times \mathbb{R}^{d_{out}}$; it processes an input signal $\mathbf{f} : SO(3) \rightarrow \mathbb{R}^{d_{in}}$ with d_{out} layer filters, each of which is defined as $\psi : SO(3) \rightarrow \mathbb{R}^{d_{in}}$ ³. Rotation-

³Note that both \mathbf{f} and ψ , and the filtered responses are defined on the domain of rotation group $SO(3)$; when the layer is the network input, \mathbf{f}

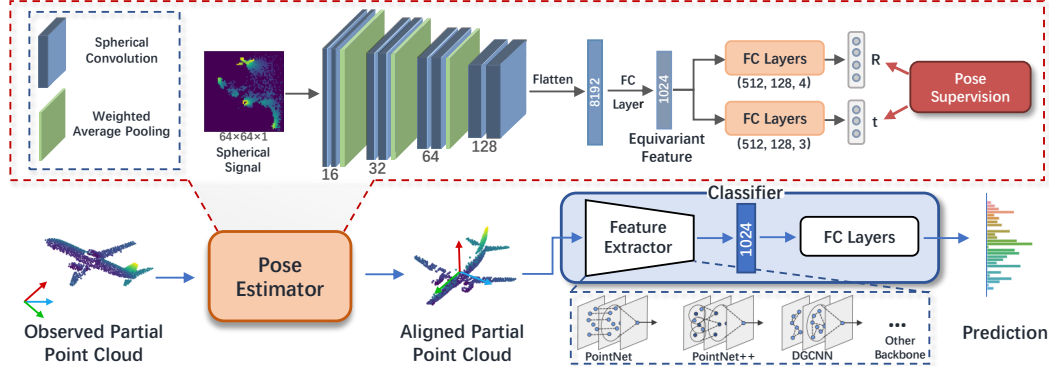


Figure 3. Pipeline of our partial point cloud classification with an auxiliary prediction of object pose in an alignment-classification manner.

equivariant Ψ has the property $[\psi \star [\mathcal{T}_R f]](Q) = [\mathcal{T}'_R [\psi \star f]](Q)$, where $Q \in SO(3)$ and \mathcal{T}_R (or \mathcal{T}'_R) denotes a rotation operator that rotates the feature function f as $[\mathcal{T}_R f](Q) = f(R^{-1}Q)$, and \star denotes convolution on the rotation group; spherical convolution defined in [6, 9] guarantees achievement of the above property. A rotation-invariant Φ_{fea} can thus be constructed by cascading multiple layers of Ψ , followed by pooling the obtained features over the domain of $SO(3)$. To implement $\Phi_{fea}(\mathcal{P})$, one may first cast each point $p \in \mathcal{P}$ onto the unit sphere, with the accompanying point-wise geometry features (e.g. the length $\|p\|_2$), and then quantize the features to the closest grid of discrete sampling on the sphere. Due to numerical approximations and the use of nonlinearities between layers, the Spherical CNN encoder is not perfectly rotation-equivariant, which will directly affect the rotation-invariance of features obtained by global pooling [28]. Alternative manners [30, 36] exist that directly learn rotation-equivariant point-wise filters in the Euclidean domain.

Weakly Supervised Learning of Spatial Transformation – Given an arbitrarily posed \mathcal{P} , a module Φ_{trans} parallel to Φ_{fea} is also considered in [23, 35, 43] to predict a transformation/pose $T = [R|t]$, which is then applied to \mathcal{P} to reduce the pose variation. Learning of Φ_{trans} is enabled by weak supervision of classification imposed on the network output of classifier Φ_{cls} , which propagates supervision signals back to Φ_{trans} . The design can be further improved via iterative updating [43, 33], similar to the point set alignment via iterative closest point [2]; it predicts a transformation update ΔT per iteration, and the one at iteration t is obtained as a composition $T_t = \prod_{i=1}^t \Delta T_i$. However, due to the weakly supervised nature, predicted T is not guaranteed to be relevant to a transformation that can align the input \mathcal{P} to its canonical pose; consequently, classification results depend empirically on data and problem settings.

Limitations with Single-View Partial Setting – The aforementioned algorithms for rotation invariance can be applied to the partial point set classification task but suffer from

the following limitations. On one hand, point sets sampled from partial object surfaces are short of the configuration of observed partial surfaces on the whole surface, which thus cannot cope with similar partial surfaces across categories effectively. On the other hand, rotation-invariant features learned from partial point sets can be less consistent. In detail, missing parts of object surfaces can lead to large feature variations, especially under different camera coordinate systems. Note that the mean coordinate of all points in the observed partial surface no longer represents the geometric center of the whole surface like the point cloud from the whole surface, which requires the network to take into account the negative effect of center deviation. Both disadvantages inhibit their classification performance in partial point cloud classification and thus encourages our solution in the following section.

5. Classification of Partial Point Clouds via an Auxiliary Object Pose Estimation

In this section, we introduce a novel classification of partial point clouds via an auxiliary prediction of object pose in a manner of alignment and classification (simply put, use an AlgCls to indicate our method), whose pipeline is illustrated in Figure 3. Specifically, the method consists of two parts – a 6D pose estimation based shape alignment module and a typical point set classifier. Instead of learning a direct mapping function $\Phi : \mathcal{X} \rightarrow \mathcal{Y}$ from partial point cloud $\mathcal{P} \in \mathcal{X}$ to the label $y \in \mathcal{Y}$, the alignment module in our method first learns a regression mapping $\Phi_{pos} : \mathcal{X} \rightarrow \mathcal{R}$ from \mathcal{P} to object pose $[R|t] \in \mathcal{R}$, whose predictions $[\hat{R}|\hat{t}]$ are utilized to transform \mathcal{P} to generate the aligned partial point clouds $\mathcal{P}' = \{p'_i \in \mathbb{R}^3\}_{i=1}^N \in \mathcal{X}'$; the latter module is to learn a classification function $\Phi_{cls} : \mathcal{X}' \rightarrow \mathcal{Y}$. Similar to the definition of a cascade function of a deep model in Sec. 4, the mapping function can be depicted as $\Phi = \Phi_{cls} \circ \Phi_{pos}$. During testing, a new partial point cloud is first fed into the shape alignment module, whose output is then used as the input of the classification module for a final class prediction.

Object Pose Estimation Based Shape Alignment – Ex-

and ψ are defined on the domain of a sphere S^2 .

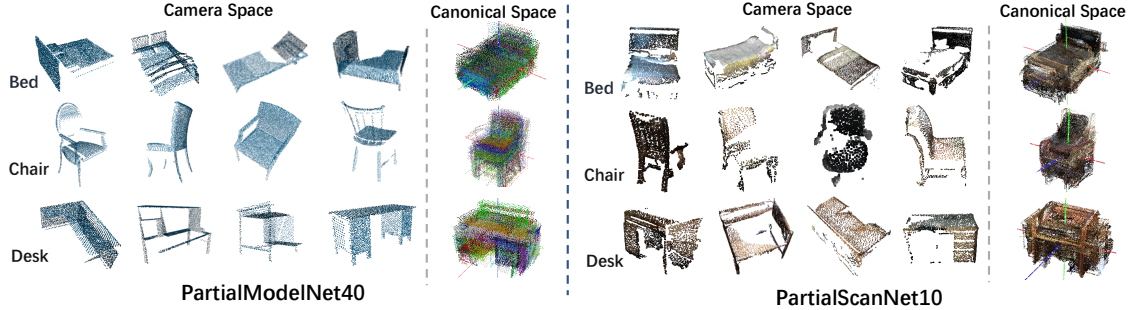


Figure 4. Illustration of the PartialModelNet40 and PartialScanNet10 datasets adapted from the ModelNet40 [37] and ScanNet [7].

isting algorithms of instance-level 6D pose estimation [38, 19, 33] typically have prior knowledge about the topological structure of object instances (*e.g.* CAD models for object instances are provided). In our setting, category-level object pose estimation is more difficult in view of shape variations. Encouraged by the recent success of Spherical CNNs [9, 6] to cope with rotation variations of the point cloud representation, this paper introduces the spherical convolution operation on partial point clouds to estimate their object poses in 6 degrees of freedom, whose rotation-equivariant features are easier to model $SO(3)$ rotation than those of the popular multi-layer perceptrons (MLPs). Note that, since the input is not a watertight mesh but a sparse and partial point cloud, we cast $W \times H$ equiangular rays from the origin and divide the whole spherical space S^2 into $W \times H$ regions. For each spherical region, we take the distance of the farthest point from the origin as the input, generating a spherical signal as $f(\theta_j, \phi_k) = d_{jk}, 1 \leq j \leq W, 1 \leq k \leq H$, where θ_j, ϕ_k denote the longitude and latitude of the region in (j, k) . In Figure 1, Spherical CNN can perform more robustly than the other methods in our partial setting, which can also verify its rationale as the feature encoder of pose regression. As shown in Figure 3, we adopt four feature encoding blocks, where the first three consists of two spherical convolution layers followed with weighted average pooling [9] and the last block only containing two spherical convolution layers as suggested by [9]. The feature map output of the final spherical convolution block is reshaped into a vector as the input of a fully-connected layer, whose output is fed into two 3-layer MLPs to predict quaternion-based rotation \hat{R} and translation \hat{t} respectively. Given pose prediction $[\hat{R}|\hat{t}]$, the original partial point cloud $\mathcal{P} = \{\mathbf{p}_i\}_{i=1}^N$ can be transformed into the aligned point set $\mathcal{P}' = \{\mathbf{p}'_i\}_{i=1}^N$ via $\mathbf{p}' = \hat{R}\mathbf{p} + \hat{t}$.

Classification of Aligned Partial Point Clouds – The aligned partial point cloud is first normalized into a unit ball as existing classifiers on complete point clouds before feeding into the point classification module. It is worth mentioning here that the classification module is not limited to a specific point cloud classifier, so any off-the-shelf classifier such as PointNet [23], PointNet++ [24], DGCNN [35] *etc.* can be adopted. In this way, the concept of the proposed

alignment-classification structure can be readily applied to any existing point-based networks to adapt from complete point cloud classification to the single-view partial setting.

Loss Functions – In our scheme, we have two types of supervision signals – the class label y and the pose label $[\mathbf{R}|\mathbf{t}] \in \mathcal{R}$. For pose estimation, the loss between ground truth and pose predictions is based on the Euclidean norm as follows:

$$L_{\text{pos}} = \|\mathbf{q} - \hat{\mathbf{q}}\| + \alpha\|\mathbf{t} - \hat{\mathbf{t}}\| \quad (1)$$

where α is the trade-off parameter between two terms, \mathbf{q} and $\hat{\mathbf{q}}$ are quaternion transformed from \mathbf{R} and $\hat{\mathbf{R}}$ respectively. For the classification loss L_{cls} , the typical cross entropy loss [23, 35] is used. In general, the total loss can be written as:

$$L_{\text{total}} = L_{\text{pos}} + \lambda L_{\text{cls}} \quad (2)$$

where λ is a trade-off parameter between the pose and classification loss.

6. Single-View Partial Point Cloud Datasets

Very few works have explored to generate and release benchmarks of partial point cloud classification, but the available datasets [37, 32] lacks object pose annotations, which cannot provide specific configuration of partial shapes. In light of this, we adapt the popular synthetic ModelNet40 [37] and realistic ScanNet [7] to the partial setting with several examples illustrated in Figure 4.

PartialModelNet40 – The ModelNet40 [37] contains 12,311 CAD models belonging to 40 semantic categories which are split into 9,843 for training and 2,468 for testing. For a PartialModelNet40 adapted from the ModelNet40, we first generate a set of pose candidates, whose rotation and translation are respectively sampled on $SO(3)$ and $t_x, t_y \sim \mathcal{U}(-2.0, 2.0), t_z \sim \mathcal{U}(2.0, 5.0)$ to simulate the operating range of a typical depth camera. In the PartialModelNet40, we respectively render 1, 5, 10 depth images with corresponding pose candidates as the pose supervision signals, from the CAD model of each instance in the training set of the ModelNet40 [37], which are then converted into partial point clouds using the intrinsic parameter of a pinhole camera. Consequently, three training split

Table 1. Comparative evaluation on classification accuracy (%) with the PartialModelNet40 and the PartialScanNet10.

Method	Input (size)	PartialModelNet40			PartialScanNet10
		1 view	5 views	10 views	
oracle [24]	pc (1024 × 3)	87.7 ± 0.1	89.9 ± 0.1	90.2 ± 0.2	91.5 ± 0.3
PointNet++ (baseline) [24]	pc (1024 × 3)	65.6 ± 0.6	67.6 ± 1.1	69.6 ± 1.0	67.7 ± 1.6
RRI [4]	pc (1024 × 3)	71.6 ± 0.1	76.2 ± 0.4	76.7 ± 0.1	71.4 ± 0.2
Spherical CNN [9]	voxel (1 × 64 ²)	71.3 ± 0.1	75.0 ± 0.4	75.1 ± 0.3	76.5 ± 0.1
STN [23]	pc (1024 × 3)	66.2 ± 1.3	69.5 ± 1.2	71.5 ± 1.0	73.1 ± 0.5
ITN [43]	pc (1024 × 3)	67.5 ± 0.6	70.1 ± 0.9	72.2 ± 0.4	66.9 ± 0.5
AlgCls (ours)	pc (1024 × 3)	73.0 ± 0.2	77.7 ± 0.3	79.7 ± 0.2	82.1 ± 0.3

include 9,843, 49,215, and 98,430 training samples. The testing set is constructed by randomly sampling one view of each testing instance in the ModelNet40, which contains 2,468 testing samples. All objects are normalized to the same size to get rid of scale variations.

PartialScanNet10 – The ScanNet [7] contains 1513 scanned and reconstructed real-world indoor scenes. Ten common semantic classes shared by the ModelNet40 and ScanNet are selected to segment partially visible instances from the scenes with bounding box annotations and semantic labels. Point cloud segments are first aligned to the canonical space using the pose annotations provided by the Scan2CAD [1], and then randomly sample five viewpoint for each object instance to transform them into the camera coordinate system. Since the original ScanNet is generated by fusing a sequence of depth scans, and thus object shapes segmenting from the ScanNet scenes evidently contain redundant surface from multiple views. In this way, the hidden point removal [14] is employed to filter out the invisible points due to self-occlusion under a single perspective. In general, our PartialScanNet10 contains 9,840 training samples and 1,695 test samples of ten categories. The PartialScanNet10 is challenging in view of the existence of realistic sensor noises, nonuniform densities, various poses, and partiality due to self-occlusion and occlusions in the cluttered context.

7. Experiments

Comparative Methods – For comparative evaluation, we choose a number of recent methods according to three types of rotation-agnostic methods in Sec. 4. For learning rotation-invariant feature representation, we choose the rigorously rotation-invariant (RRI) representation proposed in ClusterNet [4], which can achieve the state-of-the-art performance with a solid theoretical guarantee. We use the Spherical CNN [9] as a competing rotation-equivariant method, which takes the distance of the farthest point from the center in each equiangular sampling area of the bounding sphere as the spherical map feature. For a fair comparison, we select the one-branch Spherical CNN without considering the angular feature relies on the normal vector. For explicit spatial transformation, we take the spatial transformer network (STN) [23] and iterative transformer network (ITN) [43] as the baseline methods. The input

point clouds for all the methods are randomly sampled to 1024 points and normalized within the unit sphere, except for Spherical CNN [9], which uses all observed points to generate the spherical signals. We adopt the identical data preprocessing and augmentation (*i.e.* random $SO(3)$ rotation, random shift, and per-point jitter) for all the methods and report the average and variance of classification accuracy by repeating each experiment five times.

Implementation Details – We follow the default end-to-end training strategies of different classifiers suggested in their paper and insert the additional shape alignment module between input point clouds and classifiers. The hyperparameter α between rotation and translation error in Eq. (1) was empirically set as 10.0, while λ in Eq. (2) was optimally selected from $\{1, 5, 10, 20\}$. For symmetric objects, *e.g.* generalized cylinder and cuboids, we use the method proposed in [22] to map ambiguous rotations to a canonical one.

7.1. Comparative Evaluation

We compare our AlgCls method with alternative schemes using different rotation-invariance strategies on the PartialModelNet40 and PartialScanNet10. The results are shown in Table 1, and all methods except the Spherical CNN adopt the PointNet++ as the classifier.

We report the results of our method and other competitors using three training split mentioned in Sec. 6, the proposed method performs consistently the best. Both the STN and ITN can only perform comparable to or slightly outperform the baseline PointNet++, indicating that weak supervision on pose transformation can hardly tackle with the pose variation. In addition, their performance has a large variance in view of feature inconsistency without specific distribution of partial shape on the object surface. Moreover, with increasing training samples (*e.g.* from 5 views to 10 views), performance improvement of the RRI and Spherical CNN tends to saturation with a limited margin, while our method can gain a stable improvement. Our explanation for such a performance gap is that the shape alignment module in our scheme learns to transform single-view partial point clouds from arbitrary poses to the canonical ones, which thus can have consistent geometries under the unique perspective and can mitigate suffering from feature inconsistency with more training samples, while the RRI and Spherical CNN cannot in principle benefit characteriz-

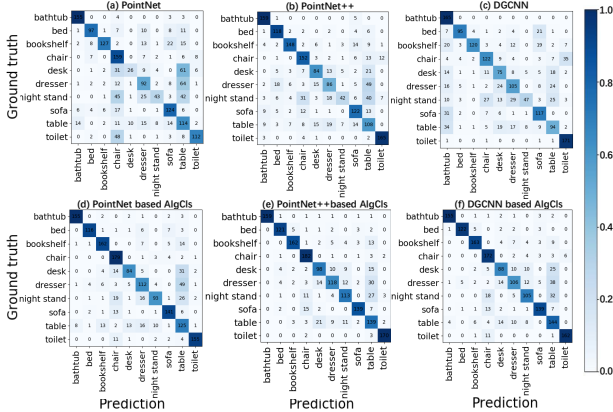


Figure 5. Confusion matrix of (a) PointNet, (b) PointNet++, (c) DGCNN, (d) PointNet based AlgCls, (e) PointNet++ based AlgCls (f) DGCNN based AlgCls on the PartialScanNet10.

Table 2. Effects of different classifiers on accuracy (%).

Dataset	PartialModelNet40 (10 views)			PartialScanNet10		
	PN	PN++	DGCNN	PN	PN++	DGCNN
Oracle	87.1	90.2	90.3	90.1	91.5	91.0
baseline	55.4	69.6	67.6	61.9	67.7	65.5
AlgCls (ours)	68.2	79.7	79.2	78.0	82.1	79.9

ing semantics with large geometric variations. Similar results on the more challenging PartialScanNet10 can be observed, and the proposed method can gain more significant performance improvement than the other rotation-agnostic methods as well as the baseline PointNet++, which further demonstrates the effectiveness of the introduction of supervised pose regression on alleviating semantic ambiguity of single-view partial point clouds. In the top row, we also report the results of our AlgCls method using ground truth pose to transform partial point clouds, which can be the upper bound of our alignment-classification algorithm based on the PointNet++ and reveals a promising direction.

7.2. Ablation Study

Effects of Different Classifiers – In Table 2 and Figure 5, we evaluate effects of different off-the-shelf classifiers, *i.e.* the PointNet (PN), the PointNet++ (PN++), and the DGCNN as the final classification Φ_{cls} module in our AlgCls on both datasets. It can be concluded that the proposed AlgCls method can consistently outperform its corresponding baseline, owing to effectively mitigating the inter-class similarity, *e.g.* the desk, dresser, and nightstand classes in Figure 5. In view of the identical classifiers adopted for Φ_{cls} as well as other settings, the performance gain can only be credited to the introduction of the shape alignment module. Moreover, among three classification methods, the PointNet++ is consistently superior to the PointNet and DGCNN, which is adopted as the default classifier of our AlgCls.

Effects of Different Feature Encoding Backbone in Shape Alignment – As mentioned in Sec. 5, we select Spherical CNN in favor of rotation equivariant properties of

Table 3. Effects of different feature encoders in pose estimation in terms of $10cm10^\circ$ metric on the PartialModelNet40 (10 views).

Backbone	PointNet	PointNet++	Spherical CNN
Accuracy (%)	6.08	11.59	26.78

spherical convolution in [9], but the PointNet architecture is adopted in explicit spatial transformation-based methods – the STN and ITN. In Table 3, we evaluate the performance of the shape alignment module in our AlgCls when using the PointNet, PointNet++, and Spherical CNN as the backbone. We report the average precision of object instances for which the error is less than $10cm$ for translation and 10° for rotation similar to [19, 34] and do not penalize rotation errors on the axis of symmetry by following [34]. The results show that the rotation equivariant features by Spherical CNN are more conducive to supervised pose estimation.

Table 4. Effects of different losses in pose estimation in terms of $10cm10^\circ$ metric on the PartialModelNet40 (10 views).

Loss	PMLoss	GeoLoss	RegLoss
Accuracy (%)	6.36	13.82	26.78

Effects of Different Pose Losses – Beyond RegLoss indicating ordinary L2 norm between pose labels and predictions, we also consider geodesic distance (GeoLoss) [11, 13] and also Point Matching Loss (PMLoss) in [19]. We report our investigation of using these losses to supervising pose estimation in Table 4, and the L2 norm based perform the best.

Table 5. Classification accuracy for different λ in Eq. (2)

λ	1.0	5.0	10.0	20.0
Accuracy (%)	79.2	79.4	79.7	78.9

Hyper-parameter λ Tuning – Table 5 shows the classification accuracy for different λ on the PartialModelNet40 (with the 10 views split). Since the classification of partial point clouds dependent on the quality of output of shape alignment but can under-fit the classification task, which suggests a relatively larger λ . According to Table 5, $\lambda = 10.0$ is used in all experiments.

8. Conclusions

This paper introduces a novel single-view partial point cloud classification from a practical perspective. To specify the distribution of partial shape on the whole surface, we propose an alignment-classification algorithm to effectively cope with additional semantic ambiguity of local primitives, which is generic to adapt other point classifiers readily to the single-view partial setting. Experiment results on two new partial point cloud datasets show that the Spherical CNN for pose estimation based shape alignment is preferred and the PointNet++ as the classifier can consistently perform best.

Acknowledgements

This work is supported in part by the National Natural Science Foundation of China (Grant No.: 61771201, 61902131), the Program for Guangdong Introducing Innovative and Entrepreneurial Teams (Grant No.: 2017ZT07X183), the Fundamental Research Funds for the Central Universities (Grant No.: 2019MS022), and the Xinhua Scholar Program of the South China University of Technology (Grant No.: D6192110).

References

- [1] A. Avetisyan, M. Dahnert, A. Dai, M. Savva, A. X. Chang, and M. Nießner. Scan2cad: Learning cad model alignment in rgb-d scans. *CVPR*, 2019. 7
- [2] P. Besl and N. D. McKay. A method for registration of 3-d shapes. *PAMI*, 1992. 5
- [3] A. X. Chang, T. Funkhouser, L. Guibas, P. Hanrahan, Q. Huang, Z. Li, S. Savarese, M. Savva, S. Song, H. Su, J. Xiao, L. Yi, and F. Yu. Shapenet: An information-rich 3d model repository. *ArXiv*, 2015. 1
- [4] C. Chen, G. Li, R. Xu, T. Chen, M. Wang, and L. Lin. Clusternet: Deep hierarchical cluster network with rigorously rotation-invariant representation for point cloud analysis. In *CVPR*, 2019. 1, 2, 3, 4, 7
- [5] D. Chen, J. Li, and K. Xu. Learning canonical shape space for category-level 6d object pose and size estimation. *CVPR*, 2020. 3
- [6] T. Cohen, M. Geiger, J. Köhler, and M. Welling. Spherical cnns. *ArXiv*, 2018. 2, 3, 4, 5, 6
- [7] A. Dai, A. X. Chang, M. Savva, M. Halber, T. Funkhouser, and M. Nießner. Scannet: Richly-annotated 3d reconstructions of indoor scenes. *CVPR*, 2017. 2, 3, 6, 7
- [8] Y. Duan, Y. Zheng, J. Lu, J. Zhou, and Q. Tian. Structural relational reasoning of point clouds. *CVPR*, 2019. 2
- [9] C. Esteves, C. Allen-Blanchette, A. Makadia, and K. Daniilidis. Learning so(3) equivariant representations with spherical cnns. In *ECCV*, 2018. 1, 2, 3, 4, 5, 6, 7, 8
- [10] A. Geiger, P. Lenz, and R. Urtasun. Are we ready for autonomous driving? the kitti vision benchmark suite. In *CVPR*, 2012. 2
- [11] R. Hartley, J. Trumpf, Y. Dai, and H. Li. Rotation averaging. *IJCV*, 2012. 8
- [12] B. S. Hua, Q. H. Pham, D. Nguyen, M. Tran, L. F. Yu, and S. Yeung. Scenenn: A scene meshes dataset with annotations. *3DV*, 2016. 3
- [13] D. Huynh. Metrics for 3d rotations: Comparison and analysis. *Journal of Mathematical Imaging and Vision*, 2009. 8
- [14] S. Katz, A. Tal, and R. Basri. Direct visibility of point sets. *TOG*, 2007. 7
- [15] A. Komarichev, Z. Zhong, and J. Hua. A-cnn: Annularly convolutional neural networks on point clouds. *CVPR*, 2019. 2
- [16] S. Lan, R. Yu, G. Yu, and L. S. Davis. Modeling local geometric structure of 3d point clouds using geo-cnn. In *CVPR*, 2019. 2
- [17] J. Li, B. Chen, and G. H. Lee. So-net: Self-organizing network for point cloud analysis. In *CVPR*, 2018. 2, 3
- [18] Y. Li, R. Bu, M. Sun, W. Wu, X. Di, and B. Chen. Pointcnn: convolution on x-transformed points. In *NeurIPS*, 2018. 2
- [19] Y. Li, G. Wang, X. Ji, Y. Xiang, and D. Fox. Deepim: Deep iterative matching for 6d pose estimation. *IJCV*, 2019. 3, 6, 8
- [20] A. Petrelli and L. D. Stefano. On the repeatability of the local reference frame for partial shape matching. In *ICCV*, 2011. 4
- [21] A. Petrelli and L. D. Stefano. A repeatable and efficient canonical reference for surface matching. In *Second International Conference on 3d Imaging*, 2012. 4
- [22] G. Pitteri, M. Ramamonjisoa, S. Ilic, and V. Lepetit. On object symmetries and 6d pose estimation from images. *3DV*, 2019. 7
- [23] C. R. Qi, H. Su, K. Mo, and L. J. Guibas. Pointnet: Deep learning on point sets for 3d classification and segmentation. *CVPR*, 2016. 1, 2, 3, 5, 6, 7
- [24] C. R. Qi, L. Yi, H. Su, and L. J. Guibas. Pointnet++: Deep hierarchical feature learning on point sets in a metric space. *NeurIPS*, 2017. 1, 2, 3, 4, 6, 7
- [25] N. Sedaghat, M. Zolfaghari, and T. Brox. Orientation-boosted voxel nets for 3d object recognition. *ArXiv*, 2017. 1
- [26] Y. Shen, C. Feng, Y. Yang, and D. Tian. Mining point cloud local structures by kernel correlation and graph pooling. *CVPR*, 2018. 2
- [27] S. Song, S. P. Lichtenberg, and J. Xiao. Sun rgb-d: A rgb-d scene understanding benchmark suite. *CVPR*, 2015. 2
- [28] R. Spzialetti, S. Salti, and L. D. Stefano. Learning an effective equivariant 3d descriptor without supervision. In *ICCV*, 2019. 5
- [29] H. Thomas, C. R. Qi, J. E. Deschaud, B. Marcotegui, F. Goulette, and L. J. Guibas. Kpconv: Flexible and deformable convolution for point clouds. *ICCV*, 2019. 2
- [30] N. Thomas, T. Smidt, S. M. Kearnes, L. Yang, L. Li, K. Kohlhoff, and P. Riley. Tensor field networks: Rotation- and translation-equivariant neural networks for 3d point clouds. *ArXiv*, 2018. 5
- [31] M. Tian, M. Ang, and G. H. Lee. Shape prior deformation for categorical 6d object pose and size estimation. In *ECCV*, 2020. 3
- [32] M. A. Uy, Q. H. Pham, B. S. Hua, D. Nguyen, and S. Yeung. Revisiting point cloud classification: A new benchmark dataset and classification model on real-world data. *ICCV*, 2019. 3, 6
- [33] C. Wang, D. Xu, Y. Zhu, R. Martín-Martín, C. Lu, L. Fei-Fei, and S. Savarese. Densefusion: 6d object pose estimation by iterative dense fusion. *CVPR*, 2019. 3, 5, 6
- [34] H. Wang, S. Sridhar, J. Huang, J. Valentin, S. Song, and L. Guibas. Normalized object coordinate space for category-level 6d object pose and size estimation. *CVPR*, 2019. 3, 8
- [35] Y. Wang, Y. Sun, Z. Liu, S. Sarma, M. Bronstein, and J. Solomon. Dynamic graph cnn for learning on point clouds. *TOG*, 2019. 1, 2, 3, 4, 5, 6

- [36] M. Weiler, M. Geiger, M. Welling, W. Boomsma, and T. Cohen. 3d steerable cnns: Learning rotationally equivariant features in volumetric data. In *NeurIPS*, 2018. 5
- [37] Z. Wu, S. Song, A. Khosla, F. Yu, L. Zhang, X. Tang, and J. Xiao. 3d shapenets: A deep representation for volumetric shapes. *CVPR*, 2015. 1, 2, 4, 6
- [38] Y. Xiang, T. Schmidt, V. Narayanan, and D. Fox. Posecnn: A convolutional neural network for 6d object pose estimation in cluttered scenes. *ArXiv*, 2018. 3, 6
- [39] Z. Xu, K. Chen, and K. Jia. W-posenet: Dense correspondence regularized pixel pair pose regression. *ArXiv*, 2019. 3
- [40] X. Yan, C. Zheng, Z. Li, S. Wang, and S. Cui. Pointasnl: Robust point clouds processing using nonlocal neural networks with adaptive sampling. *CVPR*, 2020. 2
- [41] J. Yang, Q. Zhang, B. Ni, L. Li, J. Liu, M. Zhou, and Q. Tian. Modeling point clouds with self-attention and gumbel subset sampling. *CVPR*, 2019. 2
- [42] Y. You, Y. Lou, Q. Liu, Y. Tai, L. Ma, C. Lu, and W. Wang. Pointwise rotation-invariant network with adaptive sampling and 3d spherical voxel convolution. In *AAAI*, 2020. 1, 3, 4
- [43] W. Yuan, D. Held, C. Mertz, and M. Hebert. Iterative transformer network for 3d point cloud. *ArXiv*, 2018. 2, 3, 5, 7
- [44] Z. Zhang, B. Hua, D. W. Rosen, and S. Yeung. Rotation invariant convolutions for 3d point clouds deep learning. In *3DV*, 2019. 1, 3, 4
- [45] C. Zhao, J. Yang, X. Xiong, A. Zhu, Z. Cao, and X. Li. Rotation invariant point cloud classification: Where local geometry meets global topology. *ArXiv*, 2019. 4
- [46] H. Zhao, L. Jiang, C. W. Fu, and J. Jia. PointWeb: Enhancing local neighborhood features for point cloud processing. In *CVPR*, 2019. 2
- [8] Y. Duan, Y. Zheng, J. Lu, J. Zhou, and Q. Tian. Structural relational reasoning of point clouds. *CVPR*, 2019. 2
- [9] C. Esteves, C. Allen-Blanchette, A. Makadia, and K. Daniilidis. Learning so(3) equivariant representations with spherical cnns. In *ECCV*, 2018. 1, 2, 3, 4, 5, 6, 7, 8
- [10] A. Geiger, P. Lenz, and R. Urtasun. Are we ready for autonomous driving? the kitti vision benchmark suite. In *CVPR*, 2012. 2
- [11] R. Hartley, J. Trumpf, Y. Dai, and H. Li. Rotation averaging. *IJCV*, 2012. 8
- [12] B. S. Hua, Q. H. Pham, D. Nguyen, M. Tran, L. F. Yu, and S. Yeung. Scenenn: A scene meshes dataset with annotations. *3DV*, 2016. 3
- [13] D. Huynh. Metrics for 3d rotations: Comparison and analysis. *Journal of Mathematical Imaging and Vision*, 2009. 8
- [14] S. Katz, A. Tal, and R. Basri. Direct visibility of point sets. *TOG*, 2007. 7
- [15] A. Komarichev, Z. Zhong, and J. Hua. A-cnn: Annularly convolutional neural networks on point clouds. *CVPR*, 2019. 2
- [16] S. Lan, R. Yu, G. Yu, and L. S. Davis. Modeling local geometric structure of 3d point clouds using geo-cnn. In *CVPR*, 2019. 2
- [17] J. Li, B. Chen, and G. H. Lee. So-net: Self-organizing network for point cloud analysis. In *CVPR*, 2018. 2, 3
- [18] Y. Li, R. Bu, M. Sun, W. Wu, X. Di, and B. Chen. Pointcnn: convolution on x-transformed points. In *NeurIPS*, 2018. 2
- [19] Y. Li, G. Wang, X. Ji, Y. Xiang, and D. Fox. Deepim: Deep iterative matching for 6d pose estimation. *IJCV*, 2019. 3, 6, 8
- [20] A. Petrelli and L. D. Stefano. On the repeatability of the local reference frame for partial shape matching. In *ICCV*, 2011. 4
- [21] A. Petrelli and L. D. Stefano. A repeatable and efficient canonical reference for surface matching. In *Second International Conference on 3d Imaging*, 2012. 4
- [22] G. Pitteri, M. Ramamonjisoa, S. Ilic, and V. Lepetit. On object symmetries and 6d pose estimation from images. *3DV*, 2019. 7
- [23] C. R. Qi, H. Su, K. Mo, and L. J. Guibas. Pointnet: Deep learning on point sets for 3d classification and segmentation. *CVPR*, 2016. 1, 2, 3, 5, 6, 7
- [24] C. R. Qi, L. Yi, H. Su, and L. J. Guibas. Pointnet++: Deep hierarchical feature learning on point sets in a metric space. *NeurIPS*, 2017. 1, 2, 3, 4, 6, 7
- [25] N. Sedaghat, M. Zolfaghari, and T. Brox. Orientation-boosted voxel nets for 3d object recognition. *ArXiv*, 2017. 1
- [26] Y. Shen, C. Feng, Y. Yang, and D. Tian. Mining point cloud local structures by kernel correlation and graph pooling. *CVPR*, 2018. 2
- [27] S. Song, S. P. Lichtenberg, and J. Xiao. Sun rgb-d: A rgb-d scene understanding benchmark suite. *CVPR*, 2015. 2
- [28] R. Spzialetti, S. Salti, and L. D. Stefano. Learning an effective equivariant 3d descriptor without supervision. In *ICCV*, 2019. 5

References

- [1] A. Avetisyan, M. Dahnert, A. Dai, M. Savva, A. X. Chang, and M. Nießner. Scan2cad: Learning cad model alignment in rgb-d scans. *CVPR*, 2019. 7
- [2] P. Besl and N. D. McKay. A method for registration of 3-d shapes. *PAMI*, 1992. 5
- [3] A. X. Chang, T. Funkhouser, L. Guibas, P. Hanrahan, Q. Huang, Z. Li, S. Savarese, M. Savva, S. Song, H. Su, J. Xiao, L. Yi, and F. Yu. Shapenet: An information-rich 3d model repository. *ArXiv*, 2015. 1
- [4] C. Chen, G. Li, R. Xu, T. Chen, M. Wang, and L. Lin. Clusternet: Deep hierarchical cluster network with rigorously rotation-invariant representation for point cloud analysis. In *CVPR*, 2019. 1, 2, 3, 4, 7
- [5] D. Chen, J. Li, and K. Xu. Learning canonical shape space for category-level 6d object pose and size estimation. *CVPR*, 2020. 3
- [6] T. Cohen, M. Geiger, J. Köhler, and M. Welling. Spherical cnns. *ArXiv*, 2018. 2, 3, 4, 5, 6
- [7] A. Dai, A. X. Chang, M. Savva, M. Halber, T. Funkhouser, and M. Nießner. Scannet: Richly-annotated 3d reconstructions of indoor scenes. *CVPR*, 2017. 2, 3, 6, 7

- [29] H. Thomas, C. R. Qi, J. E. Deschaud, B. Marcotegui, F. Goulette, and L. J. Guibas. Kpconv: Flexible and deformable convolution for point clouds. *ICCV*, 2019. 2
- [30] N. Thomas, T. Smidt, S. M. Kearnes, L. Yang, L. Li, K. Kohlhoff, and P. Riley. Tensor field networks: Rotation- and translation-equivariant neural networks for 3d point clouds. *ArXiv*, 2018. 5
- [31] M. Tian, M. Ang, and G. H. Lee. Shape prior deformation for categorical 6d object pose and size estimation. In *ECCV*, 2020. 3
- [32] M. A. Uy, Q. H. Pham, B. S. Hua, D. Nguyen, and S. Yeung. Revisiting point cloud classification: A new benchmark dataset and classification model on real-world data. *ICCV*, 2019. 3, 6
- [33] C. Wang, D. Xu, Y. Zhu, R. Martín-Martín, C. Lu, L. Fei-Fei, and S. Savarese. Densefusion: 6d object pose estimation by iterative dense fusion. *CVPR*, 2019. 3, 5, 6
- [34] H. Wang, S. Sridhar, J. Huang, J. Valentin, S. Song, and L. Guibas. Normalized object coordinate space for category-level 6d object pose and size estimation. *CVPR*, 2019. 3, 8
- [35] Y. Wang, Y. Sun, Z. Liu, S. Sarma, M. Bronstein, and J. Solomon. Dynamic graph cnn for learning on point clouds. *TOG*, 2019. 1, 2, 3, 4, 5, 6
- [36] M. Weiler, M. Geiger, M. Welling, W. Boomsma, and T. Cohen. 3d steerable cnns: Learning rotationally equivariant features in volumetric data. In *NeurIPS*, 2018. 5
- [37] Z. Wu, S. Song, A. Khosla, F. Yu, L. Zhang, X. Tang, and J. Xiao. 3d shapenets: A deep representation for volumetric shapes. *CVPR*, 2015. 1, 2, 4, 6
- [38] Y. Xiang, T. Schmidt, V. Narayanan, and D. Fox. Posecnn: A convolutional neural network for 6d object pose estimation in cluttered scenes. *ArXiv*, 2018. 3, 6
- [39] Z. Xu, K. Chen, and K. Jia. W-posenet: Dense correspondence regularized pixel pair pose regression. *ArXiv*, 2019. 3
- [40] X. Yan, C. Zheng, Z. Li, S. Wang, and S. Cui. Pointasnl: Robust point clouds processing using nonlocal neural networks with adaptive sampling. *CVPR*, 2020. 2
- [41] J. Yang, Q. Zhang, B. Ni, L. Li, J. Liu, M. Zhou, and Q. Tian. Modeling point clouds with self-attention and gumbel subset sampling. *CVPR*, 2019. 2
- [42] Y. You, Y. Lou, Q. Liu, Y. Tai, L. Ma, C. Lu, and W. Wang. Pointwise rotation-invariant network with adaptive sampling and 3d spherical voxel convolution. In *AAAI*, 2020. 1, 3, 4
- [43] W. Yuan, D. Held, C. Mertz, and M. Hebert. Iterative transformer network for 3d point cloud. *ArXiv*, 2018. 2, 3, 5, 7
- [44] Z. Zhang, B. Hua, D. W. Rosen, and S. Yeung. Rotation invariant convolutions for 3d point clouds deep learning. In *3DV*, 2019. 1, 3, 4
- [45] C. Zhao, J. Yang, X. Xiong, A. Zhu, Z. Cao, and X. Li. Rotation invariant point cloud classification: Where local geometry meets global topology. *ArXiv*, 2019. 4
- [46] H. Zhao, L. Jiang, C. W. Fu, and J. Jia. PointWeb: Enhancing local neighborhood features for point cloud processing. In *CVPR*, 2019. 2